Nuclear Inst. and Methods in Physics Research, A 988 (2021) 164904

Contents lists available at ScienceDirect

Nuclear Inst. and Methods in Physics Research, A

journal homepage: www.elsevier.com/locate/nima

Magnetic characterization of Mumetal® for passive shielding of stray fields down to the nano-Tesla level

Pasquale Arpaia [a,*], Philip Nicholas Burrows [b], Marco Buzio [c], Chetan Gohil [b,d], Mariano Pentella [c,e], Daniel Schulte [d]

[a] Department of Electrical Engineering and Information Technology, University of Naples "Federico II", 80138 Naples, Italy
[b] John Adams Institute (JAI), University of Oxford, Oxford, OX1 3RD, United Kingdom
[c] Technology Department, European Organization for Nuclear Research (CERN), 1211 Geneva, Switzerland
[d] Beams Department, European Organization for Nuclear Research (CERN), 1211 Geneva, Switzerland
[e] Department of Applied Science and Technology, Polytechnic of Turin, 10129, Turin, Italy

ARTICLE INFO

Keywords:
CLIC
Compact Linear Collider
Stray magnetic fields
Magnetic shielding
Magnetic materials
Mumetal®

ABSTRACT

The luminosity of a particle collider is an extremely crucial performance parameter describing its capability of producing interactions in the collision point. However, imperfections in a collider can lead to luminosity loss. Among different imperfections, an important one is stray magnetic fields. For the Compact Linear Collider (CLIC), a collider being considered as one of the main options in Europe after the Large Hadron Collider, simulations showed an unprecedented sensitivity of the machine to fields on the order of 0.1 nT. Hence, such tight constraints require special design considerations to prevent performance loss. Different shielding techniques are available in the literature, typically relying on an active shielding strategy and capable of reducing the magnetic field amplitudes down to the nano-Tesla level. However, measuring fields with such amplitudes is challenging by using state-of-the-art commercially available sensors and therefore, a passive shielding strategy, consisting in enveloping sections of the beamline with a magnetic shield, is a more attractive option. For CLIC, Mumetal®, a Ni–Fe alloy with advertised relative permeability above 100,000, was chosen. In this paper, the DC and AC magnetic characterization of two samples of Mumetal®, one annealed in its final form and the other one non-annealed is presented, showcasing how the annealing results in a boost of the magnetic permeability of more than order of magnitude. As a case study, the shielding performance of a 1-mm thin layer of Mumetal® enveloping CLIC's beamline is estimated.

1. Introduction

The Compact Linear Collider (CLIC) [1,2] is one of the main options for a collider in Europe after the Large Hadron Collider. It is a TeV-scale linear electron–positron collider currently being studied by the CLIC Collaboration. CLIC adopts a staged approach with three center-of-mass energies: 380 GeV, 1.5 TeV, and 3 TeV. The first stage is optimized for particle physics studies of the Higgs boson and top quark [3,4]. The high-energy stages will focus on direct and indirect searches for beyond Standard Model physics as well as studies of rare Standard Model processes [5].

The ability of a collider to produce interactions is characterized by its luminosity, which for head-on collisions is given by [6]:

$$\mathcal{L} = \frac{N^2 f_{\mathrm{rep}} n_b}{4\pi\sigma_x\sigma_y} H_D, \tag{1}$$

where N is the bunch population, f_{rep} is the train repetition frequency, n_b is the number of bunches per train, σ_x (σ_y) is the horizontal (vertical) beam size at the collision point and H_D is a luminosity enhancement factor due to the electromagnetic interaction of the colliding bunches. A high luminosity is desired to study rare interactions. This is achieved by targeting nanometer vertical beam sizes at the collision point. The beam size is determined by the lattice (or 'optics'), which is the arrangement of magnets installed in the accelerator, and an intrinsic property of the beam known as the emittance. The beam size and emittance are related by [7]:

$$\sigma_u = \sqrt{\epsilon_u \beta_u}, \tag{2}$$

where $u = x$ or y, ϵ_u is the geometric emittance and β_u is the beta function. Realizing a nanometer beam size relies on the production and transport of ultra-low emittance beams.

Imperfections in a collider can lead to luminosity loss. This can occur via two mechanisms: by deflecting the beams so that they collide with a relative offset or by causing emittance growth. An important imperfection in CLIC is stray magnetic fields, which can have a significant

* Corresponding author.
E-mail address: pasquale.arpaia@unina.it (P. Arpaia).

https://doi.org/10.1016/j.nima.2020.164904
Received 16 July 2020; Received in revised form 15 October 2020; Accepted 26 November 2020
Available online 5 December 2020

impact on the luminosity. Simulations [8–11] show that the beam is sensitive to stray magnetic field amplitudes on the order of 0.1 nT. This is an unprecedented sensitivity for an accelerator, which means stray magnetic fields are a serious design consideration for CLIC. A similar problem can be found in the design of experiments seeking to measure the neutron electric dipole moment [12,13] or at the Cornell Electron Storage Ring [14].

Measurements of stray magnetic fields at CERN are presented in [9, 11,15]. The measured level is several orders of magnitude above the 0.1 nT tolerance defined in [8]. This means that a dedicated system will be needed to mitigate the impact of stray magnetic fields.

A general overview of magnetic shielding techniques is described in [16]. There are two potential mitigation systems: an active compensation device, which measures the magnetic field and uses a set of coils to compensate it or a passive magnetic shielding system. An active system was used in [17] to stabilize a magnetic field to fluctuations of less than 10 nT. Another solution capable of shielding a magnetic field to the nano-Tesla level is presented in [18]. However, an active compensation device relies on accurately measuring the magnetic field. Measuring magnetic field amplitudes of 0.1 nT is challenging with current commercially available sensors [19]. For instance, Superconducting Quantum Interference Devices (SQUIDs) were used in biomedical applications such as magnetocardiography (MCG) [20], where an attenuation up to 10 pT was reached by using an rf-SQUID-based setup. However, the adoption of this setup is impractical on a large scale machine such as CLIC. Therefore, the passive shielding strategy is a more attractive option.

A passive shielding strategy involves enveloping sections of the beamline with a magnetic shield, which would prevent the stray magnetic fields from reaching the beam. There are two mechanisms for magnetic shielding [21]:

- Flux-shunting, where the magnetic field is drawn into the material, which diverts it away from the shielded region.
- Eddy-current cancellation, where a time-varying magnetic field induces a current in the material, which produces a magnetic field that opposes the original magnetic field.

The eddy-current cancellation mechanism is effective for shielding high-frequency magnetic fields, whereas the flux-shunting mechanism for low frequencies [21]. The eddy-current cancellation mechanism results in losses in the material. For CLIC, passive shielding can be used to target low-frequency stray magnetic fields, which means the flux-shunting mechanism is more important and eddy-current losses in the material are less important.

In this paper, the magnetic properties of a material that can be used for this purpose, known as Mumetal® are presented. Alternative materials proposed in the literature include superconducting shields [22,23]. However, superconducting materials have the serious drawback of requiring very low temperatures to operate. As CLIC is a normal conducting machine, the use of a superconducting shield is unappealing.

Conventional ferromagnetic steels (i.e. low-carbon steels, silicon steels, etc.) having lower magnetic permeability (on the order of 5000) and higher saturation point (at least twice higher) would provide poor performance, given the extremely low amplitude of the stray fields to be shielded. In fact, they are more suitable for fields above 1 T, where Mumetal® is saturated and therefore results transparent to the field. For fields below 1 T, instead, Mumetal® is not saturated and the much higher advertised permeability values determine shielding performance not achievable with a conventional ferromagnetic steel.

Mumetal® has been used to shield superconducting RF cavities from static magnetic fields [24,25] and shield a beam from magnetic field pulses at the Fermi National Accelerator Laboratory [26]. These applications focused on shielding static magnetic fields or pulses that last for a few seconds. For CLIC, the concern is dynamic magnetic fields with frequencies up to a few kHz.

Table 1
Nominal data of Mumetal® from [28], referred to a fully annealed state material.

Parameter	DC	AC (60 Hz)
Saturation flux density B_s	0.74 T	0.74 T
Coercive field H_c	<1.59 A/m	<1.59 A/m
Initial@L@ relative permeability (at $B = 4$ mT)	50,000	100,000
μ_r at H = 0.4 A/m	150,000	250,000
Maximum relative permeability μ_r	350,000	350,000

The goal of this paper is to verify if the magnetic properties of Mumetal® are suitable for stray field shielding in CLIC and, more generally, for applications well below the nano-Tesla level. In particular, Section 2 presents the magnetic characterization of two test specimens, one annealed and the other one not annealed. The material magnetic characterization was carried out to validate the vendor supplied data. The data from Section 2, finally, are used in Section 3 to assess the shielding performance in the Compact Linear Collider by using numeric simulations.

2. Material magnetic properties

2.1. Mumetal® specifications and sample preparation

Mumetal® is a particular supermalloy, an iron–nickel alloy with an 80 % nickel content. The high nickel content leads to a relative permeability above 100,000 and a coercive field on the order of 1 A/m [27]. This permeability value allows better shielding performance in comparison with other ferromagnetic materials. A small amount of additional elements such as molybdenum, silicon and manganese is also added to stabilize the material lattice. These elements constitute a few percent of the material composition.

The material properties of Mumetal® must be characterized to estimate its shielding performance. Moreover, data supplied by the manufacturer may differ significantly from the measured ones or data at the field levels or the frequencies of the desired application may be missing. Two-mu metal samples with identical chemical composition (80% Ni, 5% Mo, 15% Fe, 0.3–0.5% Mn and 0.1–0.4% Si) produced by the Magnetic Shield Corporation, USA [28] were tested. Table 1 reports the nominal values from the data sheet for comparison with the measured one.

These samples were prepared as follows:

1. A toroid formed from 22 Mumetal® laminations. Each layer has a thickness of 0.2 mm, giving a total thickness of 4.4 mm. The laminations were coated with magnesium methylate. This sample was annealed in its final form by the vendor, who did not disclose any detail.
2. A toroid formed from annealed Mumetal® foil of thickness 0.1 mm. The laminations were not coated. The toroid was formed by stacking 17 rings, giving a total thickness of 1.7 mm. This sample was not annealed in its final form.

Each sample has an inner and outer diameter of 105 mm and 114 mm respectively and they were put inside a holder made of bluestone. Finally, two coils were wound around the holder: the innermost one of 90 turns and the outermost with 13 turns. Fig. 1 shows a cross-section of the test specimen layout.

2.2. Measurement method

The two samples were measured by means of the flux-metric method [29,30], a transformer-based method whose measurement system layout is shown in Fig. 2.

The toroidal specimen is wound with two coils: a N_e turns excitation coil which carries the current responsible for the generation of

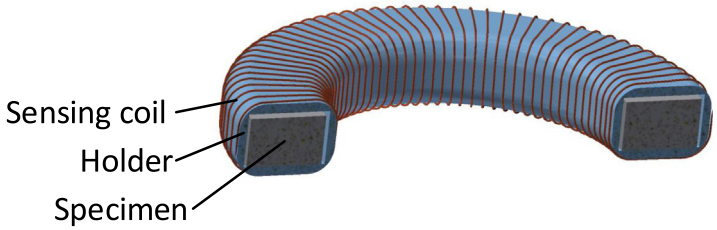

Fig. 1. Test specimen layout: the sample (gray) is contained inside the holder (blue). The coils are both wound around the holder to avoid mechanical stress on the sample. (For interpretation of the references to color in this figure legend, the reader is referred to the web version of this article.)

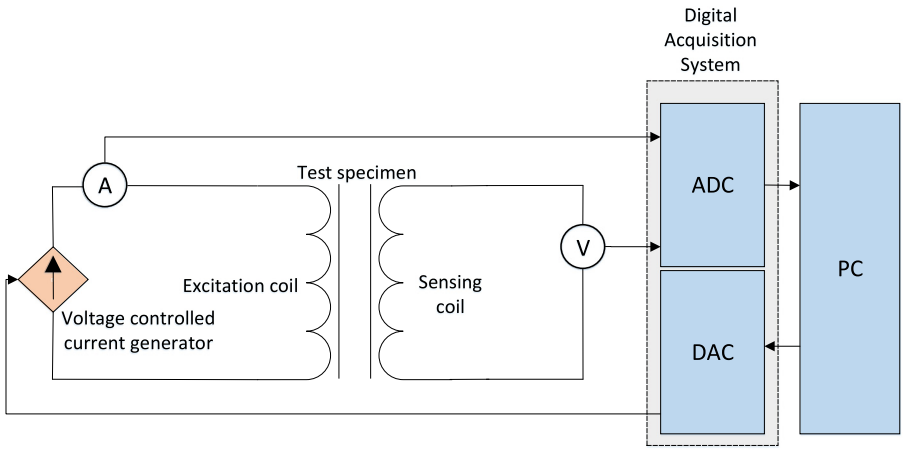

Fig. 2. Measurement system layout.

magnetic field H to be applied to the material and a N_t turns sensing coil which detects the voltage due to the magnetic flux variations.

The Digital Acquisition System (DAQ) monitors the whole measurement process by continuously recording current and voltage and by generating the reference signal for the voltage-controlled current generator that powers the excitation coil.

The magnetic field H is assumed uniform within the sample cross-section and evaluated from the measurement of the current i:

$$H = \frac{N_e i}{2\pi r_0}, \tag{3}$$

where r_0 is the log-mean radius of the test specimen. The magnetic flux linked with the N_t sensing turns, Φ, is obtained by integration of the induced voltage v:

$$\Phi = \int_{t_0}^{t} v(\tau) d\tau \tag{4}$$

The initial value is neglected because the specimen is demagnetized before the measurement. Considering the ratio between the outer and inner diameter less than 1.1 in compliance with the standard, the magnetic flux density distribution within the sample cross-section can be assumed equal to the one of the magnetic field and therefore is evaluated as:

$$B = \frac{1}{A_s}\left(\frac{\Phi(t)}{N_t} - \mu_0 H A_a\right), \tag{5}$$

where A_s is the cross-sectional area of the sample, $A_a = A_t - A_s$ is the part of the cross-sectional area occupied by air, A_t is the cross-sectional area of the sensing coil, $\mu_0 H A_a$ is the air-flux compensation and μ_0 is the permeability of the free space.

2.3. DC magnetic properties

The DC magnetic properties were retrieved by applying the *point-by-point* method as described by the IEC 60404-4 standard [31]. The current is ramped back and forth between positive and negative symmetric values. Each ramp is followed by a plateau where the current is kept constant to damp the eddy currents. The plateau amplitude is increased at each cycle. The points of the initial magnetization curve $(H_k B_k)$ corresponds to the peak point of the nested hysteresis loops. The points of the relative permeability curve, μ_{rk} are retrieved by the following formula:

$$\mu_{rk} = \frac{B_k}{\mu_0 H_k}. \tag{6}$$

Fig. 3 shows the measured initial magnetization curve and corresponding relative permeability for each sample.

The two samples show different magnetic properties. Sample 1 displays a permeability peak of roughly 415,000, whereas the peak permeability of sample 2 is roughly 14,000. The initial permeability for samples 1 and 2 are 50,000 and 5,000 respectively. At the maximum field levels, sample 2 does not reach saturation, whereas sample 1 becomes completely saturated.

The higher permeability for sample 1 is suspected to be due to the annealing process of the specimen in its final form and the absence of mechanical strain in the sample. The different saturation behavior could be explained by the different stacking conditions: sample 2 was not annealed in its final form and some mechanical strain may have been applied when stacking the rings in the sample holder.

The major hysteresis loop was measured in compliance with the standard [31] by ramping the current back and forth between two symmetric current values with no plateaux and such that the material is brought to the saturation region. The overall duration of the excitation cycle was 60 s. Fig. 4 shows the two major hysteresis loops.

Although the sample are made from the same material, they display completely different hysteresis loops. Sample 2 has a coercive field of 6.89 A/m whilst sample one has a coercive field of 1.27 A/m. Moreover, as shown in Fig. 3, although the saturation flux density is the same in both cases, the approach to the saturation region is different with sample 1 saturating at fields 10 times lower than sample 2. The

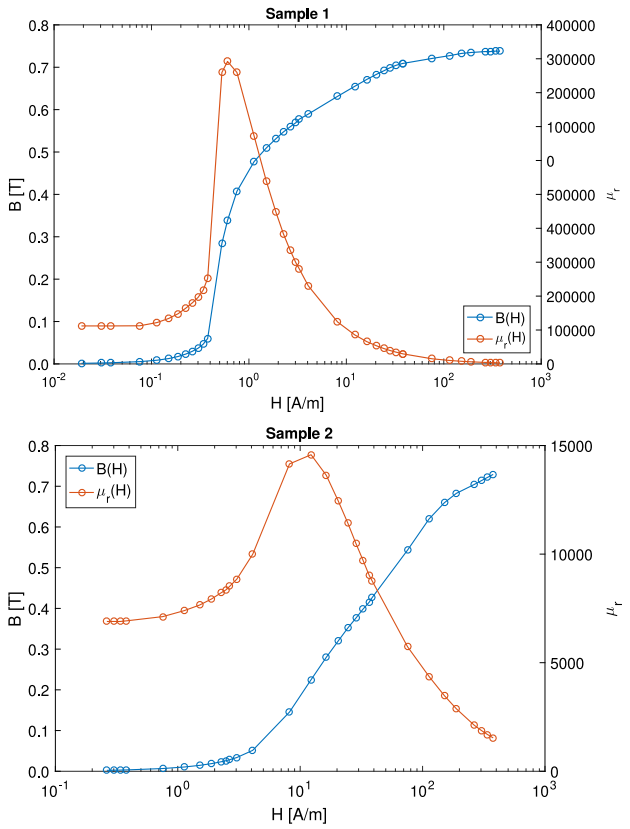

Fig. 3. Measured points of the initial magnetization curve (blue, left axis) and relative permeability values as a function of the applied field (red, right axis) for the two samples. (For interpretation of the references to color in this figure legend, the reader is referred to the web version of this article.)

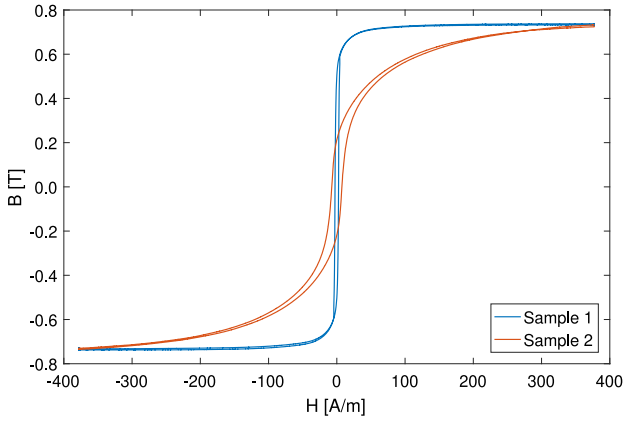

Fig. 4. Measured DC hysteresis loops for the two Mumetal® samples.

comparison between the measurements of sample 1 and the nominal data reported in Table 1 shows no significant variations.

2.4. AC magnetic properties

The effectiveness of Mumetal® in shielding dynamic magnetic fields depends strongly on its AC magnetic properties. The AC data reported in Table 1 are incomplete because only the properties at 60 Hz are reported. Moreover, considering the higher reported values of the relative permeability, those data are referred to a relation between the peak points of H and B from the test cycle, as suggested by the standard [32], with B ideally increasing with the frequency. The

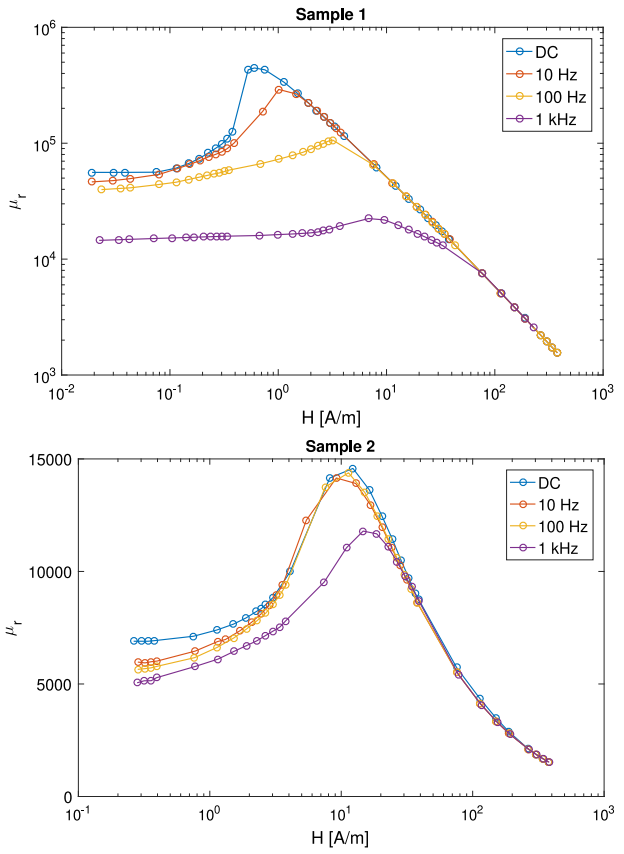

Fig. 5. Measured AC permeability values as a function of the externally applied field for different frequency values for sample 1 (top) and 2 (bottom).

initial magnetization curves evaluated in the following are measured according to a different criterion, consisting in evaluating the points that maximize the energy density. In this way, the increasing phase shift between H and B, dependent on the frequency, is considered to better represent the field weakening due to the eddy currents circulation. The relationship between H and B, therefore, will be represented by an apparent relative permeability that takes intrinsically into account the skin depth.

The AC magnetic properties of the two samples were measured in the range 1–1000 Hz, at 10 frequency values per decade. A fixed-frequency sinusoidal waveform was used for the excitation current. The amplitude of the waveform was increased after each cycle.

Fig. 5 shows the relative permeability as a function of the magnetic field at three different frequencies for both samples. The DC curve was added for comparison.

Fig. 6 shows the peak permeability and initial permeability as a function of the frequency for each sample. Sample 1 is more sensitive to frequency than sample 2. The peak permeability of sample 1 at 1 kHz drops by approximately 95 % with respect to the DC value. Sample 2 exhibits a drop in the peak permeability of only 20 % with respect to the DC value. The changes in the relative permeability become appreciable for sample 2 only above 200 Hz. The permeability of both samples decreases roughly proportionally to $1/f$.

The same trend can also be observed in the initial permeability. Sample 1 shows an initial permeability that decreases from 43,730 to 13,470 (a reduction of approximately 70 %). Sample 2, on the other hand, displays an initial permeability that decreases from 5,580 to 4,690 (a reduction of approximately 16 %).

Fig. 7 shows the hysteresis loop at different frequencies for the two samples. The hysteresis loops follow consistently the behavior seen in terms of relative permeability. Sample 1 is strongly affected by the

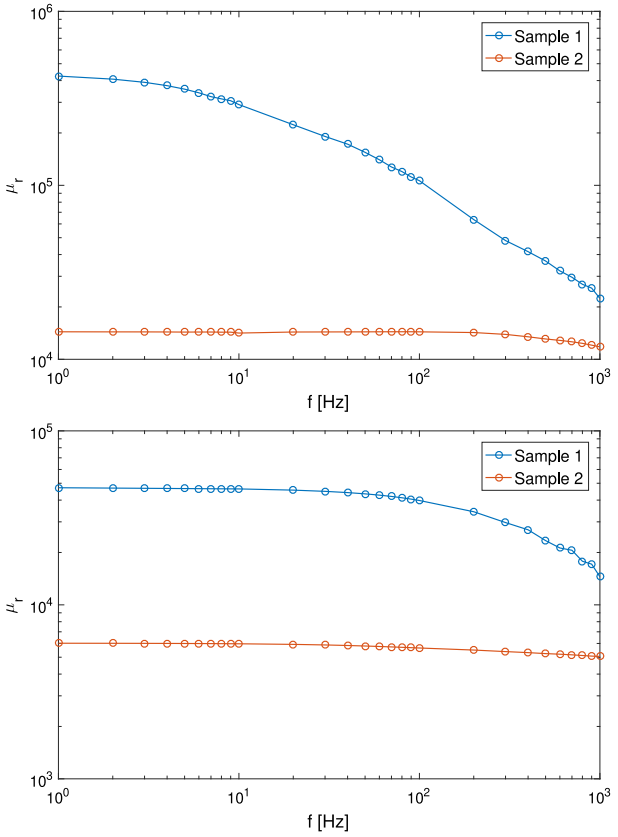

Fig. 6. Measured AC peak (top) and initial (bottom) permeability values as a function of the frequency for the two samples.

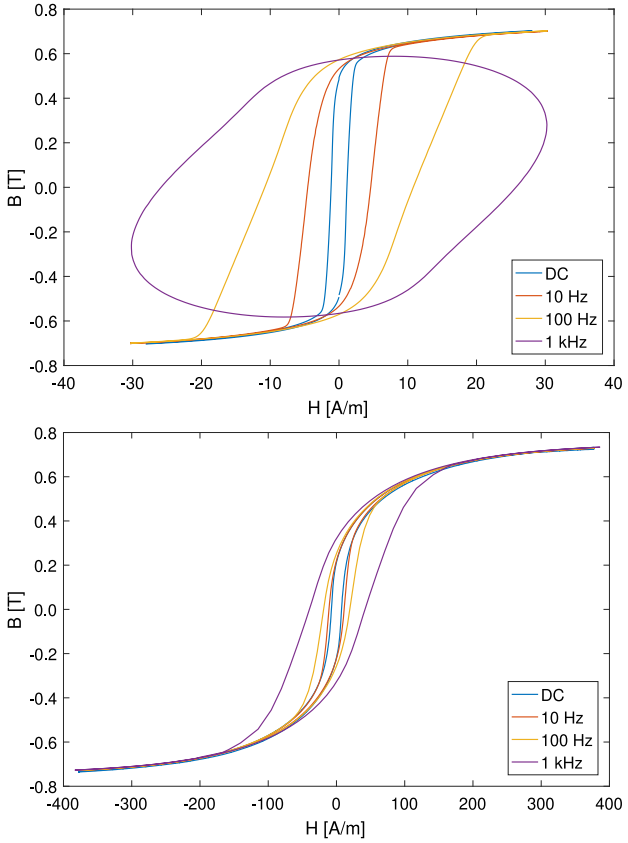

Fig. 7. Measured hysteresis loops for sample 1 (top) and 2 (bottom) at different frequency values. The loops are respectively shown at different field levels for the two samples to highlight the changes in the saturation region.

eddy current screening and at 1 kHz the effect of saturation is no longer visible, with the loop largely dominated by the eddy-current field contributions. Sample 2 shows approximately the same relative variation as sample 1 in terms the coercive field but does not display the widening of the hysteresis loop due to the eddy currents.

3. Mumetal® Shielding in CLIC

The concern for CLIC is small-amplitude stray magnetic fields, which are on the order of nT at frequencies below 1 kHz. These stray fields reduce the quality of the beam. The impact of stray fields on the CLIC beam is described in detail in [33]. The main effect is due to the influence of stray fields in long drift sections. In the 380 GeV stage of CLIC, one of the most sensitive regions is a 3.5 km long transfer line, which has a FODO cell lattice with 218.4 m long drifts [1]. The proposed mitigation method is to envelop drift sections with a magnetic shield to prevent the stray fields from reaching the beam. A thin layer of Mumetal® can be added around the beam pipe in drifts for shielding. Beam pipes are usually cylindrical in shape with diameters of a few centimeters. A typical beam pipe consists of a few millimeters of steel and a 10–100 μm inner copper coating [1]. In this work, a radius of 1 cm for the CLIC beam pipe is assumed.

3.1. Shielding model

As the length of the beam pipe is several orders of magnitude higher than the diameter, the magnetic shield was modeled as an infinitely long cylinder and end effects were neglected. Analytical solutions exist for the shielding factor of a cylindrical magnetic shield. Simple formulae for a cylindrical Mumetal® shield can be found in [34]. An approximate formula for the shielding factor of a single layer ferromagnetic shield is given by [34]:

$$S = \frac{\mu_r t}{D}, \tag{7}$$

where t is the thickness of the shield and D is its diameter. The key material property that determines the shielding factor is the permeability. Eq. (7) describes shielding via the flux-shunting mechanism and does not include any additional shielding via the eddy-current cancellation mechanism.

In this paper, the exact solution to Maxwell's equations for the propagation of electromagnetic waves through a magnetic shield is calculated with the methodology outlined in [35]. The model in [35] includes both the flux-shunting and eddy-current cancellation shielding mechanisms. To calculate the shielding factor the permeability must be specified as a function of frequency for the expected stray field amplitude in the CLIC tunnel. As the material relative permeability at the expected stray field amplitudes is constant, the permeability only needs to be specified as a function of the frequency because it is reasonable to assume it constant as the field decreases.

3.2. Shielding performance

The CLEAR (CERN Linear Electron Accelerator for Research) facility is the closest representation of a CLIC-like beamline at CERN. The ambient magnetic field was measured at several locations in CLEAR [15]. The magnetic field was measured in three orthogonal directions and the Power Spectral Density (PSD) of the vector sum was considered. Fig. 8 shows the largest magnetic field PSD measured in CLEAR (in black). A description of the features in the PSD can be found in [15]. A worst-case scenario was assumed, where the entire PSD corresponds to

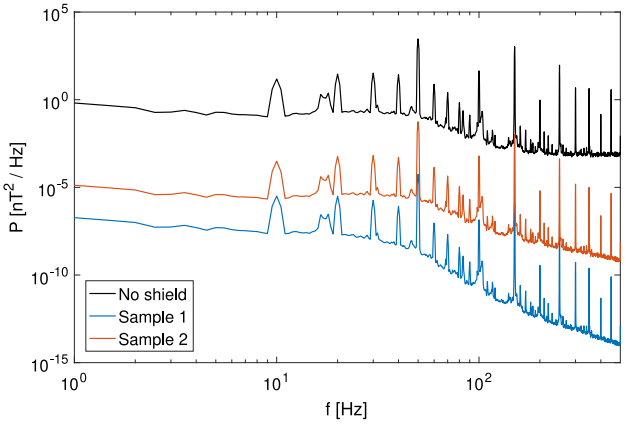

Fig. 8. Largest magnetic field PSD (sum of all three components) measured in CLEAR [15] (black) and the impact of a 1 mm Mumetal® shield formed from each sample (blue and red). (For interpretation of the references to color in this figure legend, the reader is referred to the web version of this article.)

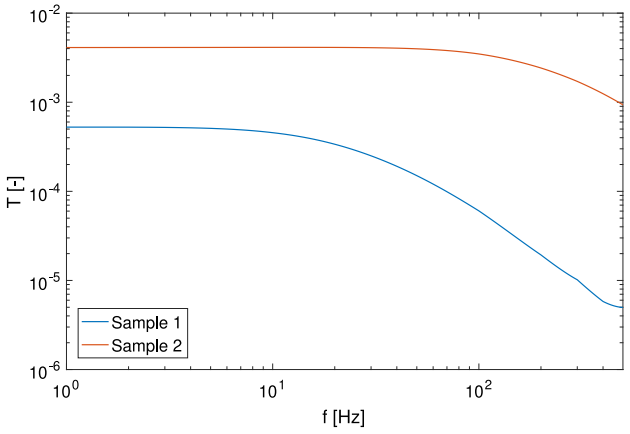

Fig. 9. Transfer function for the two Mumetal® samples evaluated by using the measured initial permeability.

the magnetic field in a transverse direction with respect to the beam. This PSD was used as an estimate of the level of stray fields CLIC could experience. The PSD of the magnetic field inside a shield $P(f)$ can be calculated as:

$$P(f) = |T(f)|^2 P_0(f), \tag{8}$$

where $P_0(f)$ is the PSD of the magnetic field outside the shield and $T(f)$ is the transfer function of the shield.

Fig. 9 shows the transfer function calculated with the methodology presented in [35] for the two Mumetal® samples. The Mumetal® shield was modeled as a cylinder with an inner radius of 1 cm and thickness of 1 mm. The permeability in Fig. 6 (bottom) was used in this calculation. The transfer function begins to diminish at higher frequencies despite the lower permeability due to shielding from the eddy-current cancellation mechanism. The impact of a shield formed from the two samples on the PSD measured in CLEAR is shown in Fig. 8.

The integral of a PSD gives the variance. This property can be used to calculate the standard deviation as a function of the frequency range:

$$\sigma(f) = \sqrt{\int_f^\infty P(f')\,\mathrm{d}f'}. \tag{9}$$

Plotting the standard deviation as a function of frequency is helpful to examine the frequency content of the stray field. Fig. 10 shows the standard deviation of the magnetic field measured in CLEAR including

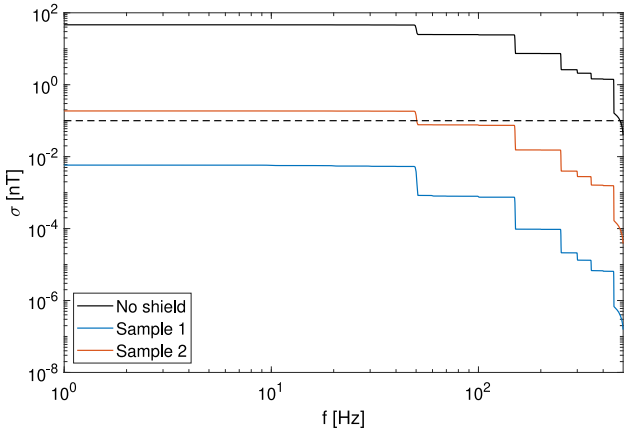

Fig. 10. Standard deviation of the magnetic field measured in CLEAR (black) and the impact of a 1 mm Mumetal® shield formed from each sample (red and blue). The dashed line shows the required tolerance level. (For interpretation of the references to color in this figure legend, the reader is referred to the web version of this article.)

Table 2
Standard deviation of the magnetic field (given to two significant figures) measured in CLEAR and standard deviation of the magnetic field in presence of a 1 mm Mumetal® shield formed from each sample.

Shield	Standard deviation [nT]
No shield	46
Sample 1	5.8×10^{-3}
Sample 2	0.19

the effect of a Mumetal® shield formed from each sample. The standard deviation for each case is summarized in Table 2. Without a magnetic shield the stray field is several orders of magnitude above the 0.1 nT tolerance defined in [8]. A 1 mm Mumetal® shield formed from sample 2 is not effective enough to reduce the standard deviation to less than 0.1 nT. A Mumetal® shield formed from sample 1 is extremely effective, which reduces the standard deviation to a pT level.

4. Conclusions

In this paper, the importance of stray magnetic fields shielding has been highlighted in order to show its importance in terms of impact on a collider performance. In particular, for CLIC, an approach based on passive shielding of sections of the beamline by Mumetal® has been preferred as a more attractive alternative to other techniques (i.e. active compensation) and materials (i.e. superconducting shields).

Afterward, the DC and AC properties of Mumetal® were characterized up to a frequency of 1 kHz with magnetic field amplitudes up to roughly 350 A/m. Two specimens were tested: one annealed in its final form and the other one non-annealed. The results showed that the annealing determines a boost in the relative permeability of more than one order magnitude. The frequency response of the two samples is also different, with the annealed one presenting a drop of 70–95 % in the apparent permeability, whereas the non-annealed one is much less sensitive to the frequency. Hence, the boost in the magnetic permeability resulting from the annealing determines a much stronger field weakening effect within the material cross-section and therefore, better shielding performance.

As a case study, the magnetic properties of the two samples were used to evaluate the shielding performance of the material for CLIC, a proposed future e^+e^- collider that is sensitive to stray magnetic fields to a pico-Tesla level. A 0.1 nT tolerance was defined in [8]. The proposed solution to mitigate stray fields is to envelop sections of the beamline with Mumetal®. Using stray field measurements performance in the CLEAR facility at CERN to characterize the expected amplitude, the

results show a 1 mm annealed Mumetal® layer is enough to reduce the stray field to well below the 0.1 nT tolerance level.

An activity to be carried out in the future will be to assess the stability of the material over time. At this extremely low field levels, in fact, the effect of any change in the material properties due to temperature, humidity, microstructure, etc. might deeply impact the shielding performance. Moreover, in case of a future series production, a dedicated measurement campaign shall be dedicated to the quality control of the material production for statistical purposes.

CRediT authorship contribution statement

Pasquale Arpaia: Validation, Supervision. **Philip Nicholas Burrows:** Validation, Supervision. **Marco Buzio:** Resources, Validation, Supervision. **Chetan Gohil:** Conceptualization, Methodology, Investigation, Formal analysis, Writing - original draft, Writing - review & editing. **Mariano Pentella:** Conceptualization, Methodology, Investigation, Formal analysis, Writing - original draft, Writing - review & editing. **Daniel Schulte:** Resources, Supervision.

Declaration of competing interest

The authors declare that they have no known competing financial interests or personal relationships that could have appeared to influence the work reported in this paper.

Acknowledgments

The authors thank Magnetic Shield Co. for the provision of the specimens. They thank also CERN colleagues S. Sgobba for fruitful discussions and R.B. Mercadillo for technical support.

References

[1] M. Aicheler, P. Burrows, N. Catalan, R. Corsini, M. Draper, J. Osborne, D. Schulte, S. Stapnes, M. Stuart, The compact linear collider (CLIC)-project implementation plan, 2019, arXiv preprint arXiv:1903.08655.

[2] M. Aicheler, P. Burrows, M. Draper, T. Garvey, P. Lebrun, K. Peach, N. Phinney, H. Schmickler, D. Schulte, N. Toge, A Multi-TeV Linear Collider Based on CLIC Technology: CLIC Conceptual Design Report, CERN Yellow Reports: Monographs, CERN, Geneva, 2012, http://dx.doi.org/10.5170/CERN-2012-007, URL http://cds.cern.ch/record/1500095.

[3] H. Abramowicz, A. Abusleme, K. Afanaciev, N.A. Tehrani, C. Balázs, Y. Benhammou, M. Benoit, B. Bilki, J.-J. Blaising, M. Boland, et al., Higgs physics at the CLIC electron-positron linear collider, Eur. Phys. J. C 77 (7) (2017) 475.

[4] H. Abramowicz, N.A. Tehrani, D. Arominski, Y. Benhammou, M. Benoit, J.-J. Blaising, M. Boronat, O. Borysov, R. Bosley, I.B. Jelisavčić, et al., Top-quark physics at the CLIC electron-positron linear collider, J. High Energy Phys. 2019 (11) (2019) 3.

[5] J. De Blas, R. Franceschini, F. Riva, P. Roloff, U. Schnoor, M. Spannowsky, J. Wells, A. Wulzer, J. Zupan, S. Alipour-Fard, et al., The CLIC potential for new physics, 2018, arXiv preprint arXiv:1812.02093.

[6] K. Yokoya, P. Chen, Beam-beam phenomena in linear colliders, in: Frontiers of Particle Beams: Intensity Limitations, Springer, 1992, pp. 415–445.

[7] E. Wilson, E.J. Wilson, An Introduction to Particle Accelerators, Clarendon Press, 2001.

[8] C. Gohil, D. Schulte, P.N. Burrows, Stray Magnetic Field Tolerances for the 380 Gev CLIC Design, Tech. Rep. CERN-ACC-2018-0052. CLIC-Note-1139, CERN, Geneva, 2018, URL http://cds.cern.ch/record/2649488.

[9] C. Gohil, P. Burrows, M. Buzio, E. Marín, D. Schulte, Measurements and Impact of Stray Fields on the 380 GeV Design of CLIC, CERN-ACC-2018-089. CLIC-Note-1150, 2018, http://dx.doi.org/10.18429/JACoW-IPAC2018-THPAF047, THPAF047. 4 p. URL http://cds.cern.ch/record/2653716.

[10] J. Snuverink, W. Herr, C. Jach, J. Jeanneret, D. Schulte, F. Stulle, Impact of Dynamic Magnetic fields on the CLIC Main Beam, CERN-ATS-2010-083. CLIC-Note-840, 2010, 3 p. URL http://cds.cern.ch/record/1271359.

[11] E. Marin, B. Heilig, J. Pfingstner, D. Schulte, Impact of Dynamical Stray Fields on CLIC, CERN-ACC-2017-134. CLIC-Note-1116, 2017, http://dx.doi.org/10.18429/JACoW-IPAC2017-MOPIK077, MOPIK077. 4 p. URL http://cds.cern.ch/record/2289695.

[12] T. Andalib, J. Martin, C. Bidinosti, R. Mammei, B. Jamieson, M. Lang, T. Kikawa, Sensitivity of fields generated within magnetically shielded volumes to changes in magnetic permeability, Nucl. Instrum. Methods Phys. Res. A 867 (2017) 139–147.

[13] J.W. Martin, R.R. Mammei, W. Klassen, C. Cerasani, T. Andalib, C.P. Bidinosti, M. Lang, D. Ostapchuk, Large magnetic shielding factor measured by nonlinear magneto-optical rotation, Nucl. Instrum. Methods Phys. Res. A 778 (2015) 61–66.

[14] W. Hartung, D. Asner, J. Conway, C. Dennett, S. Greenwald, J.-S. Kim, Y. Li, T. Moore, V. Omanovic, M. Palmer, et al., In-situ measurements of the secondary electron yield in an accelerator environment: Instrumentation and methods, Nucl. Instrum. Methods Phys. Res. A 783 (2015) 95–109.

[15] C. Gohil, N. Blaskovic Kraljevic, P.N. Burrows, B. Heilig, D. Schulte, Measurements of stray magnetic fields at CERN for CLIC, in: 10th Int. Partile Accelerator Conf., IPAC'19, Melbourne, Australia, 19–24 May 2019, JACOW Publishing, Geneva, Switzerland, 2019, pp. 289–292.

[16] T. Sumner, J. Pendlebury, K. Smith, Convectional magnetic shielding, J. Phys. D: Appl. Phys. 20 (9) (1987) 1095.

[17] D. Spemann, T. Reinert, J. Vogt, J. Wassermann, T. Butz, Active compensation of stray magnetic fields at LIPSION, Nucl. Instrum. Methods Phys. Res. B 210 (2003) 79–84.

[18] T. Bryś, S. Czekaj, M. Daum, P. Fierlinger, D. George, R. Henneck, M. Kasprzak, K. Kirch, M. Kuźniak, G. Kuehne, et al., Magnetic field stabilization for magnetically shielded volumes by external field coils, Nucl. Instrum. Methods Phys. Res. A 554 (1–3) (2005) 527–539.

[19] P. Ripka, M. Janosek, Advances in magnetic field sensors, IEEE Sens. J. 10 (6) (2010) 1108–1116.

[20] F. Shanehsazzadeh, M. Fardmanesh, Low noise active shield for SQUID-based magnetocardiography systems, IEEE Trans. Appl. Supercond. 28 (4) (2017) 1–5.

[21] S. Celozzi, R. Araneo, Electromagnetic shielding, in: Encyclopedia of RF and Microwave Engineering, Wiley Online Library, 2005.

[22] K. Capobianco-Hogan, R. Cervantes, A. Deshpande, N. Feege, T. Krahulik, J. LaBounty, R. Sekelsky, A. Adhyatman, G. Arrowsmith-Kron, B. Coe, et al., A magnetic field cloak for charged particle beams, Nucl. Instrum. Methods Phys. Res. A 877 (2018) 149–156.

[23] S. Slutsky, C. Swank, A. Biswas, R. Carr, J. Escribano, B. Filippone, W. Griffith, M. Mendenhall, N. Nouri, C. Osthelder, et al., Cryogenic magnetic coil and superconducting magnetic shield for neutron electric dipole moment searches, Nucl. Instrum. Methods Phys. Res. A 862 (2017) 36–48.

[24] M. Masuzawa, K. Tsuchiya, A. Terashima, Study of magnetic shielding materials and fabrication of magnetic shield for superconducting cavities, IEEE Trans. Appl. Supercond. 24 (3) (2013) 1–4.

[25] M. Masuzawa, K. Tsuchiya, A. Terashima, A. Dael, O. Napoly, J. Plouin, Magnetic shielding: Our experience with various shielding materials, SRF2013, Paris, France, 2013.

[26] S. Nagaitsev, C. Gattuso, S. Pruss, J. Volk, Experience with magnetic shielding of a large scale accelerator, in: PACS2001. Proceedings of the 2001 Particle Accelerator Conference (Cat. No. 01CH37268), Vol. 5, IEEE, 2001, pp. 3371–3373.

[27] F. Fiorillo, Measurement and Characterization of Magnetic Materials, North-Holland, 2004.

[28] Magnetic Shield Corporation, USA, http://www.magnetic-shield.com/index.html.

[29] A. Parrella, P. Arpaia, M. Buzio, A. Liccardo, M. Pentella, R. Principe, P. Ramos, Magnetic properties of pure iron for the upgrade of the LHC superconducting dipole and quadrupole magnets, IEEE Trans. Magn. 55 (2) (2018) 1–4.

[30] P. Arpaia, M. Buzio, S.I. Bermudez, A. Liccardo, A. Parrella, M. Pentella, P.M. Ramos, E. Stubberud, A superconducting permeameter for characterizing soft magnetic materials at high fields, IEEE Trans. Instrum. Meas. 69 (7) (2020) 4200–4209.

[31] IEC, Magnetic Materials-Part 4: Methods of Measurement of Dc Magnetic Properties of Magnetically Soft Materials, IEC, IEC 60404-4.

[32] IEC, Magnetic Materials - Part 6: Methods of Measurement of the Magnetic Properties of Magnetically Soft Metallic and Powder Materials at Frequencies in the Range 20 Hz to 100 Khz by the Use of Ring Specimens, IEC, IEC 60404-6.

[33] C. Gohil, Dynamic Imperfections in the Compact Linear Collider (DPhil thesis), University of Oxford, UK, 2020.

[34] D. Dubbers, Simple formula for multiple mu-metal shields, Nucl. Instrum. Methods Phys. Res. A 243 (2–3) (1986) 511–517.

[35] J. Hoburg, A computational methodology and results for quasistatic multilayered magnetic shielding, IEEE Trans. Electromagn. Compat. 38 (1) (1996) 92–103.